ELSEVIER Fluid Dynamics Research 26 (2000) 105–117

FLUID DYNAMICS

Coherent structures in numerically simulated jets with and without off-source heating

S.S. Siddhartha[a], R. Narasimha[b,*], A.J. Basu[b], S.V. Kailas[c]

[a] *Indian Institute of Technology Madras, Chennai 600 036, India*
[b] *Fluid Dynamics Unit, Jawaharlal Nehru Centre for Advanced Scientific Research, Bangalore 560 064, India*
[c] *Centre for Civil Aircraft Design and Development, National Aerospace Laboratories, Bangalore 560 012, India*

Received 18 January 1999; accepted 25 March 1999

Abstract

Direct numerical solutions of the incompressible Navier–Stokes equations, under the Boussinesq approximation, for the temporal evolution of a jet-like flow have been analyzed to educe coherent structures. The eduction procedure involved both conventional image processing and the application of the wavelet transform — here used as a spatially delimited filter to smooth out fine scale discontinuities and reveal the underlying order. Attention has been focussed on the vorticity and its components (azimuthal, radial and streamwise). It is found that the nature of the coherent motion is most strongly evident in the azimuthal component of the vorticity, and is revealed to consist of a toroidal base supporting a thin conical sheath; the interior of the structure is nearly devoid of azimuthal vorticity. There is some evidence of a secondary structure in the radial and streamwise components of the vorticity, which show strips of opposite sign close to each other, suggesting vortex pairs, possibly helically organized. With addition of volumetric heat after the (unheated) jet has achieved self-similarity, the structures tend to telescope into each other because of the acceleration produced by the heating, and the coherence present in the unheated jet is severely disrupted.

Keywords: Turbulent jet; Direct numerical solutions; Coherent structures; Off-source heating; Wavelet transform

1. Introduction

While the presence of large-scale organization in the turbulent mixing layer and in some other flows has been well documented, the occurrence and nature of coherent structures in the fully developed jet continues to be a matter of debate. In general, it is accepted that the nature of any coherent structure that may be present in jets is much less clear than in mixing layers. This is because while the energy in the coherent motion in mixing layers is as much as 20%, it is estimated that in the far jet it is only 10% (Fiedler, 1987).

* Corresponding author. Fax: +91-80-334-6634.
E-mail address: roddam@caos.iisc.ernet.in (R. Narasimha)

0169-5983/00/$ 20.00
PII: S0169-5983(99)00017-9

There have been several proposals on coherent structures in jet flows. It has been established beyond doubt that the near-field of a round jet is an axisymmetric mixing layer, dominated by vortex rings generated by the Kevin–Helmholtz instability. The far-field of the jet is, however, less clear. Dimotakis et al. (1983), using the laser-induced fluorescence technique for flow visualization, inferred the presence of large-scale vortical structures in the jet far-field; both axisymmetric and spiral (antisymmetric) configurations were observed. They proposed that the far-field of the jet would be in the form of an expanding spiral. Using the same technique of flow visualization, Dahm and Dimotakis (1990) reported that the instantaneous concentration field consisted of an ordered sequence of arrowhead-shaped structures, with dimensions of the order of the local width of the flow in both directions. Within each of these structures, the concentration of the mixed fluid showed only marginal variations. Dahm and Dimotakis suggested that the topological and dynamical complexity of the jet might be a consequence of simultaneous instability in both axisymmetric and helical modes, causing the flow to keep switching between the two modes. Fig. 1(a) shows the proposed instantaneous dilution pattern of Dahm and Dimotakis for the far-field of a turbulent jet; it implies that the jet fluid concentration decays in a stepwise fashion over regions of roughly uniform concentration. Direct visual observations of a high Reynolds number jet by Mungal and Hollingsworth (1989) confirmed the presence of arrowhead-shaped structures, but suggested a rather different internal structure, of the kind shown in Fig. 1(b). In this picture, upstream structures are thought to telescope into their downstream counterparts. Yoda et al. (1994), based on three-dimensional concentration measurements, proposed that the helical mode, when present, was in the form of a pair of counter-rotating spirals present simultaneously in the flow: the observed indication of a spiral in two-dimensional axial slices of the flow are to be interpreted, according to them, as slices of a simple sinusoid in three dimensions. They suggested that the two instantaneous concentration fields proposed for the axisymmetric and helical modes (Figs. 1(a) and (b), respectively), were simply slices of the same structure at different orientations. These conclusions were derived from data sets that were deliberately biased to select only those which clearly showed antisymmetric shapes with respect to the jet axis. The assumption underlying this procedure was that the helical mode, being the most unstable, shapes the concentration field in the self-similar region of the jet. A plausible argument proposed by them for the simultaneous presence of a counter-rotating pair of helices is that they could be caused by vortex reconstruction interactions between tilted near-field vortex rings.

From correlation measurements, Tso and Hussain (1989) inferred the dominant structure to be a single helix, but a double helix and a ring-like structure were also found.

The effects of off-source volumetric heating on jet flow have been studied experimentally by Elavarasan et al. (1995) and Bhat and Narasimha (1996), by use of ohmic heating in a jet of electrically conducting fluid. The results showed that heating accelerates the flow and inhibits growth. Turbulent velocities increase, but not as rapidly as mean velocities, resulting in a drop in normalized intensities. There were also indications of disruption of the structures in the flow.

In the present study, we explore the eduction of coherent structures from the direct numerical simulation (Basu and Narasimha, 1999) of a turbulent "jet-like" flow and study the effects of off-source heating on the organization of the flow. The simulation carried out was essentially a temporal analogue of the laboratory experiments of Elavarasan et al. (1995) and Bhat and Narasimha (1996), in the sense that while in the experiments heat was injected at all times in a limited streamwise region along the jet, in the simulation, heat injection occurred over a limited time in the entire

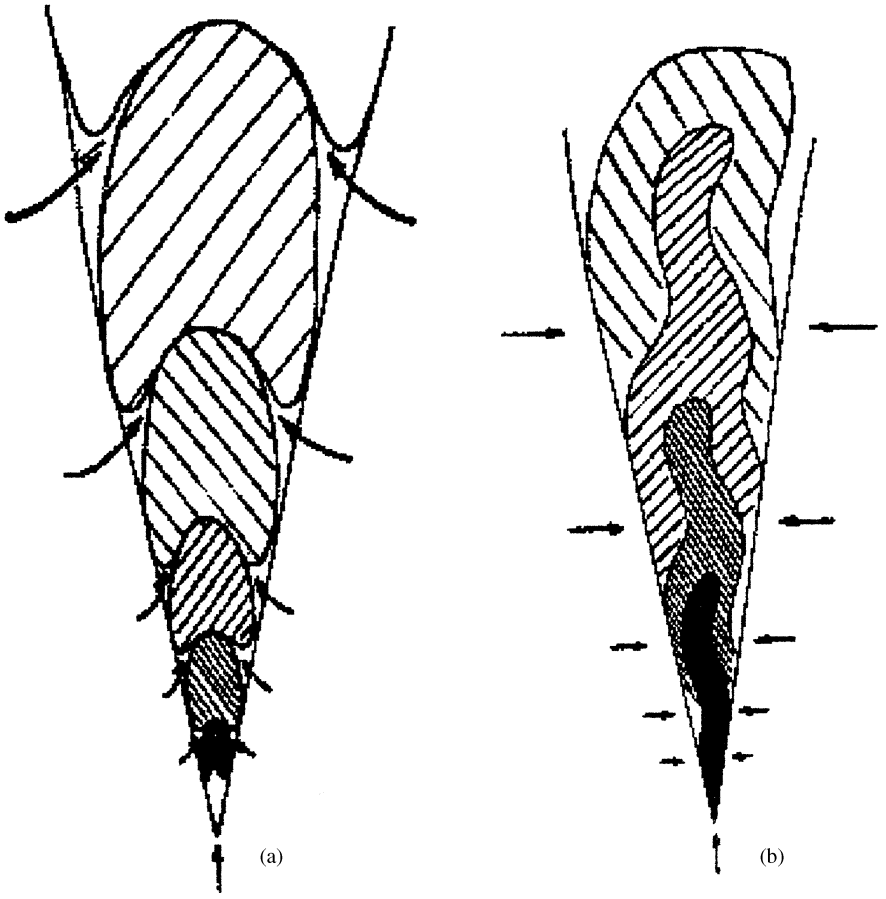

Fig. 1. Schematic of instantaneous concentration fields in a round turbulent jet, as proposed by (a) Dahm and Dimotakis, axisymmetric mode, (b) Mungal and O'Neil, helical mode. (Reproduced from Mungal and Hollingsworth, 1989).

flow (Fig. 2). The simulation thus produces a flow that, while not identical with the spatially developing jet, closely resembles it, i.e. although three-dimensional structures of the kind known to occur in a laboratory jet are captured, such events as ring-formation and pairing now occur over the temporal evolution of the flow, and not in a particular region in space. The main advantage of the numerical simulation is that the vorticity, which is the primary flow variable that defines a coherent structure, can be easily derived from numerical solutions, while it is hard to measure experimentally. We use both conventional image processing and the continuous two-dimensional wavelet transform to pick out and enhance the structure against the non-coherent background. Wavelet transforms can provide useful assistance in detecting structures in turbulent flows; this has been demonstrated on round turbulent jets by Kailas et al. (1992), and on the mixing layer by Kailas and Narasimha (1999). For our present analysis, we use wavelets for the limited purpose of smoothing out the fine-scale discontinuities in the flow and revealing the underlying large-scale organization.

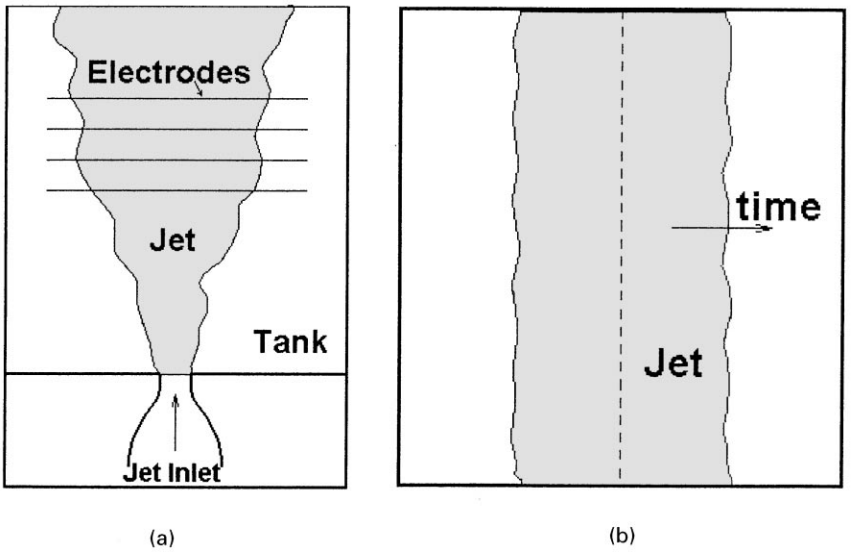

Fig. 2. Schematic of the flow: (a) Experimental jet, (b) Numerical simulation. (Reproduced from Basu and Narasimha, 1999).

2. Numerical method

Processed data was obtained from the direct numerical simulation reported by Basu and Narasimha (1999) for a cylindrical mixing layer. These simulations solve the Navier–Stokes equations with buoyancy, using the Boussinesq approximation. The Boussinesq approximation neglects the effect of density changes in the inertial terms, but includes the buoyancy force in the momentum equation. The heat injection appears as a source term in the energy equation. The equations are

$$\nabla \cdot \boldsymbol{u} = 0, \tag{2.1}$$

$$\frac{\partial \boldsymbol{u}}{\partial t} + (\boldsymbol{u} \cdot \nabla)\boldsymbol{u} = -\frac{1}{\rho}\nabla p + v\nabla^2 \boldsymbol{u} - \alpha T \boldsymbol{g}, \tag{2.2}$$

$$\frac{\partial T}{\partial t} + (\boldsymbol{u} \cdot \nabla)T = k\nabla^2 T + \frac{J}{C_p}, \tag{2.3}$$

where $\boldsymbol{u}$ is the velocity vector, ρ the density of the fluid, p the pressure, v the kinematic viscosity of the fluid, α the coefficient of thermal expansion, T the change in temperature above the ambient, $\boldsymbol{g}$ the acceleration due to gravity, k the thermal diffusivity, J the rate of head addition per unit volume, and C_p the specific heat at constant pressure.

To non-dimensionalize equations (2.1)–(2.3), the initial diameter d_0 and the initial center-line velocity U_0 of the cylindrical mixing layer, and a characteristic temperature difference T_0, were used as scales. The scale T_0 was defined as the net temperature change that would result if the total heat Jt_h, where t_h is the duration of heat injection, is injected uniformly over unit volume: $T_0 = Jt_h/C_p$.

We then get (in addition to Eq. (2.1), whose form does not change)

$$\frac{\partial T}{\partial t} + (\boldsymbol{u} \cdot \nabla)T = \frac{1}{\mathrm{Re}\,\mathrm{Pr}}\nabla^2 T + \frac{d_0}{U_0 t_\mathrm{h}} g(r), \tag{2.4}$$

$$\frac{\partial \boldsymbol{u}}{\partial t} + (\boldsymbol{u} \cdot \nabla)\boldsymbol{u} = -\nabla p + \frac{1}{\mathrm{Re}}\nabla^2 \boldsymbol{u} + GC_\mathrm{h} T, \tag{2.5}$$

where all variables are now non-dimensional, $\mathrm{Re} = U_0 d_0/\nu$ is the Reynolds number, $\mathrm{Pr} = \nu/k$ is the Prandtl number, $g(r)$ is a prescribed radial distribution function, and

$$G = \frac{g\alpha d_\mathrm{h}^2}{\rho c_p}\frac{J}{U_\mathrm{h}^3}, \tag{2.6}$$

d_h, U_h being, respectively, relevant length and velocity scales in the heating region. The heating parameter G is analogous to the non-dimensional heat release number introduced in Bhat and Narasimha (1996), except that Eq. (2.6) incorporates a modification to take account of the fact that in the present simulation the heat release occurs over a finite duration t_h in time, and not over a finite region in space as in Bhat and Narasimha (1996). Either version of G is a measure of the ratio of buoyancy to inertia forces, like the Richardson number. The other non-dimensional parameter in Eq. (2.5) is

$$C_\mathrm{h} = \frac{U_\mathrm{h} t_\mathrm{h}}{d_\mathrm{h}}\frac{d_0}{d_\mathrm{h}}\left(\frac{U_\mathrm{h}}{U_0}\right)^2, \tag{2.7}$$

whose value will remain constant during the present study. (This corresponds to fixing the spatial region over which heat is added in a real jet.) Since G and C_h appear only as a product, we use $G^* = GC_\mathrm{h}$ as the relevant non-dimensional parameter governing heat release in the present study.

Eqs. (2.1)–(2.3) were solved in a Cartesian coordinate system using the Fourier–Galerkin (spectral) technique. To facilitate the use of the spectral scheme, the boundary conditions were taken to be periodic in each space direction for all the primary variables, namely pressure, temperature and velocity.

The initial conditions for the velocity components were set up so that there was a tubular shear layer aligned vertically upwards along the z direction at $t=0$. Streamwise and azimuthal perturbations were added to expedite roll-up and the development of the Widnall instability. The initial velocity field was made divergence-free using the Helmholtz decomposition. The size of the computational domain (a periodic cubical box of dimension $L \times L \times L$) was taken to be four times the diameter of the tabular shear layer at $t = 0$.

The computations were carried out at a constant Reynolds number $\mathrm{Re} = 1600$ (based on the flow at $t = 0$), Prandlt Number $\mathrm{Pr} = 7$ and $G^* = 0.04$ using both 64^3 and 128^3 grids. The data analyzed here have all been calculated using the 128^3 grid solutions. We have used X, Y and Z to denote the pixel location along the x-, y- and z-axis of the domain, respectively. The time step used was $t = 0.0025$. This time step was halved in the heated case to resolve the finer scales that were found to be generated by heat addition. More details are available in Basu and Narasimha (1999).

The vorticity transport equation, obtained by taking the curl of Eq. (2.2), is

$$\frac{\partial \boldsymbol{\omega}}{\partial t} + (\boldsymbol{u} \cdot \nabla)\boldsymbol{\omega} - (\boldsymbol{\omega} \cdot \nabla)\boldsymbol{u} - \nu\nabla^2 \boldsymbol{\omega} = \alpha \boldsymbol{g} \times \nabla T, \tag{2.8}$$

where the terms on the left are familiar from the classical theory. The term on the right is a source of vorticity; it arises from the baroclinic torque $\nabla p \times \nabla \rho$ when the pressure gradient ∇p is replaced by its value in the hydrostatic approximation, and the density gradient $\nabla \rho$ by the temperature gradient, to which it is proportional in the approximation we are using.

3. Techniques used

The raw data for our analysis was a 128^3 grid of processed vorticity data. Sections of this grid were taken along various planes and analyzed for structures. After many trials, we found the following eduction scheme very useful.

(a) *Thresholding*: Since we wish to focus first on the large-scale structures associated with comparatively large values of vorticity, the smaller vorticities were thresholded out (i.e. set to zero if below threshold). Various thresholds were tried and the one which visually showed the greatest degree of order was chosen. By and large, this threshold did not exceed 10% of the maximum value of the vorticity, so that no significant information on the higher vorticities was lost due to thresholding.

(b) *Wavelet transform*: It was sometimes useful to apply the 2D wavelet transform to the thresholded image. For the present analysis, we have used the 2D Mexican hat wavelet,

$$\psi(\boldsymbol{x}) = (2 - x^2 + y^2) \exp - (x^2 + y^2)/2,$$

where $\boldsymbol{x} = (x, y)$ is a position vector in the plane of the image being analyzed. The zero crossings of this transform have been shown to be particularly useful in detecting regions of sharp gradient in an image (Marr and Hildreth 1980) — here, the interface between the coherent structure and its background. The computation of the wavelet transforms was accomplished using the software package NALLETS ver. 3.0, developed by SVK at the National Aerospace Laboratories, Bangalore for analysis of complex turbulence data. The scale of the transform (a') is given by the ratio of the wavelet size to the dimension of the image (here taken as 128 on each side). By using NALLETS, it was possible to vary this scale continuously from a minimum value of $\frac{11}{128}$ (determined by the minimum number of wavelet points required to satisfy the "admissibility" condition on the wavelet, see e.g. Meyer, 1993) to any arbitrarily larger scale (upto unity). We found the scale $\frac{16}{128}$ to be optimal, i.e. it was the smallest wavelet scale which visually revealed the best coherence in the structure. After the application of the transform, the image was again thresholded to trim out the smearing of the edges caused by the convolution of the wavelet over the raw data (mathematical noise). It was also found that the vorticity field could be recognized better if all the wavelet transform coefficients (WTC) beyond the selected threshold were considered as belonging to the same class (by rendering them in a single color irrespective of the sign).

4. The unheated jet

Fig. 3 (reproduced from Basu and Narasimha, 1999) shows contours of the absolute magnitude of vorticity of the fully developed jet, in the yz-plane, from times $t = 25$ to 35 in steps of two time units. The contour levels start from 0.5 with increments of 0.5.

At $t = 25$, the unheated jet is roughly cylindrical in shape. The jet boundaries are sharp, only weakly convoluted and continuous. Also, vorticity is nearly uniformly distributed throughout the jet.

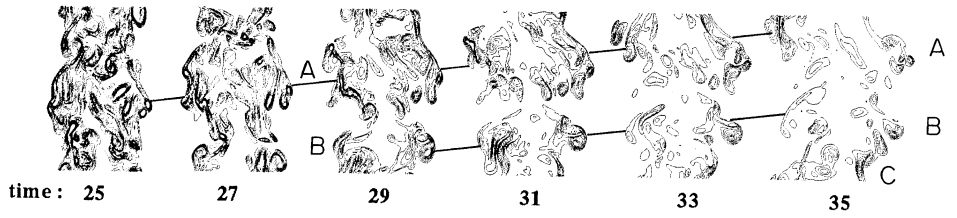

Fig. 3. Evolution of absolute magnitude of vorticity in the unheated jet at section $X = 65$ from times $t = 25$ to 35 in steps of two time units. Contour levels start from 1 with increments of 0.5.

By $t = 27$, the boundaries begin to break up and "bulges" swell out on either side of the jet axis (structure A). At $t = 29$, the bulges take the form of an "arrowhead" shaped region, very much like those observed by Dahm and Dimotakis.

Another nascent arrowhead B is seen developing at the bottom of the domain. The jet boundary is now highly convoluted. Also, the vorticity distribution is no longer uniform: patches of irrotational fluid appear near the jet axis. By $t = 35$, structure A has moved downstream from its nearly central position to the top of the box. Structure B is now at the center of the box. The distinct arrowhead shape of B is most clearly seen in this frame. A third structure C is seen developing at the bottom, but this may be seen as a continuation of A, because of the periodic boundary conditions.

For the temporally simulated unheated jet, with periodic boundary conditions, Basu and Narasimha (1999) have shown that vorticity varies with time as given by the similarity solution

$$\omega(t) \sim \frac{t^{-2/3}}{t^{1/3}} \sim t^{-1}. \tag{4.1}$$

Thus, there is a natural decay of vorticity with time. In studying the temporal evolution of the structures in the flow this decay could be misleading if the same absolute values of vorticity are used in data processing; we have found it much more convenient to analyze a normalized vorticity. If t_0 is some suitably chosen virtual origin and t_1 is some fixed time after similarity has been achieved, the similarity solution (4.1) suggests that we can write

$$(t - t_0)\omega(t) = (t_1 - t_0)\omega(t_1).$$

We find $t_0 = 15.8$ from the ω vs. t plot (Fig. 8, Basu and Narasimha, 1999) and choose $t_1 = 25$ as our reference, as by this time the jet begins to follow the similarity solution. We may thus define the normalized vorticity as

$$\omega^*(t) = \omega(t)\frac{(t - t_0)}{(25 - t_0)} = \omega(t)\frac{(t - 15.8)}{9.2}.$$

To understand the nature of the coherent structure, we have studied separately the azimuthal, radial and streamwise components of the vorticity, but find the azimuthal component most illuminating. Fig. 4 shows the axial sections at $X = 65$ of normalized azimuthal vorticity from times $t = 25$ to 35. The most striking feature is that these plots display more clearly the coherent motions revealed in the vorticity magnitude plot. Structures A–C are reproduced. Also, the azimuthal vorticity is mostly positive. Negative vorticity is generally sparse, and is confined to the central region within the jet. The structure is seen to have a thick toroidal base that supports a conical sheath of positive azimuthal vorticity around the arrowhead shaped region observed by Dahm and Dimotakis.

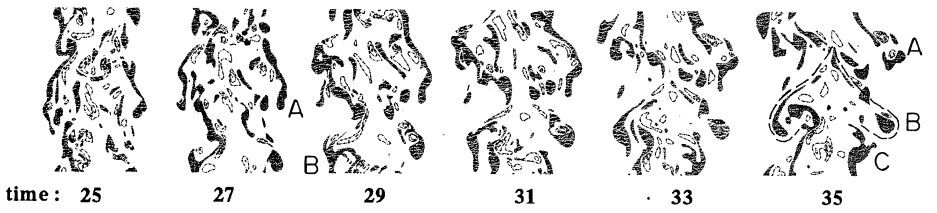

Fig. 4. Evolution of normalized azimuthal vorticity in the unheated jet at section $X = 65$ from times $t = 25$ to 35 in steps of two time units. Solid (dashed line) contours: positive (negative) values.

We now focus our attention on $t = 35$ as at this time structure B, centrally located in the domain, is visually the most coherent. Fig. 5 shows the plots of the magnitude and the azimuthal, radial and streamwise components of vorticity at $X = 65$ and time $t = 35$. It is important to note that all the plots have been given the same threshold. It is clear from Fig. 5 that the radial and streamwise plots do not have the evident coherence of the azimuthal component, and in particular there is no indication of the toroidal base and the sheath it supports. We thus conclude that the dominant large structure is coherent chiefly in the azimuthal vorticity.

There is, however, a striking feature in the radial and streamwise vorticity fields, namely that some strips of positive and negative vorticity occur in pairs at roughly the same locations in both of them. These are indicated by numbers 1–5 in the streamwise plot; $1'$, $2'$ and $5'$ are the corresponding pairs in the radial plot (Fig. 5c and d). In order to see if these could form a pattern, all the paired points in the streamwise plot may be connected, maintaining the direction of rotation and continuity of the vortex line. The resulting configuration is a distorted figure of eight roughly in the same location as the arrowhead B, shown as a dotted line in Figs. 5a and b. This suggests that the arrowhead could consist of a thick toroidal base connected to a helix on top of it, roughly as Bhat and Narasimha (1996) proposed. But this is hard to establish with greater confidence from the given data.

Fig. 6 shows the wavelet transform of the azimuthal vorticity section at $X = 65$ and time $t = 35$ at the optimal scale (Section 3) of 16/128. As discussed in Section 1, we use the wavelet here ás a spatially delimited filter — akin to moving a window over the entire image, the window averaging over whatever image is seen within it. The transform clearly brings out the continuity in the structure, which is not so easily perceptible from the raw image. The important features to be noticed here are the continuity of the outer sheath of the structure and the hollowness of the inside of the structure.

Fig. 7 shows the velocity and the wavelet transform plots at a perpendicular section at $Y = 65$ at $t = 35$. The plot reveals, not surprisingly, that structure B is not perfectly axisymmetric; compared to the section at $X = 65$, which has an onion-shaped Kremlin-type "dome", the structure at $Y = 65$ is stretched streamwise and rounded at the top. Apart from this, the other feature, namely the azimuthal sheath and the hollow interior, are identical to the $X = 65$ section. The wavelet transform, as in the previous image, brings out these features of structure B more clearly.

5. Heated jet

Fig. 8 shows time evolution of the magnitude of vorticity in the heated jet, in axial sections at $X = 65$. Heating commences at $t = 25$.

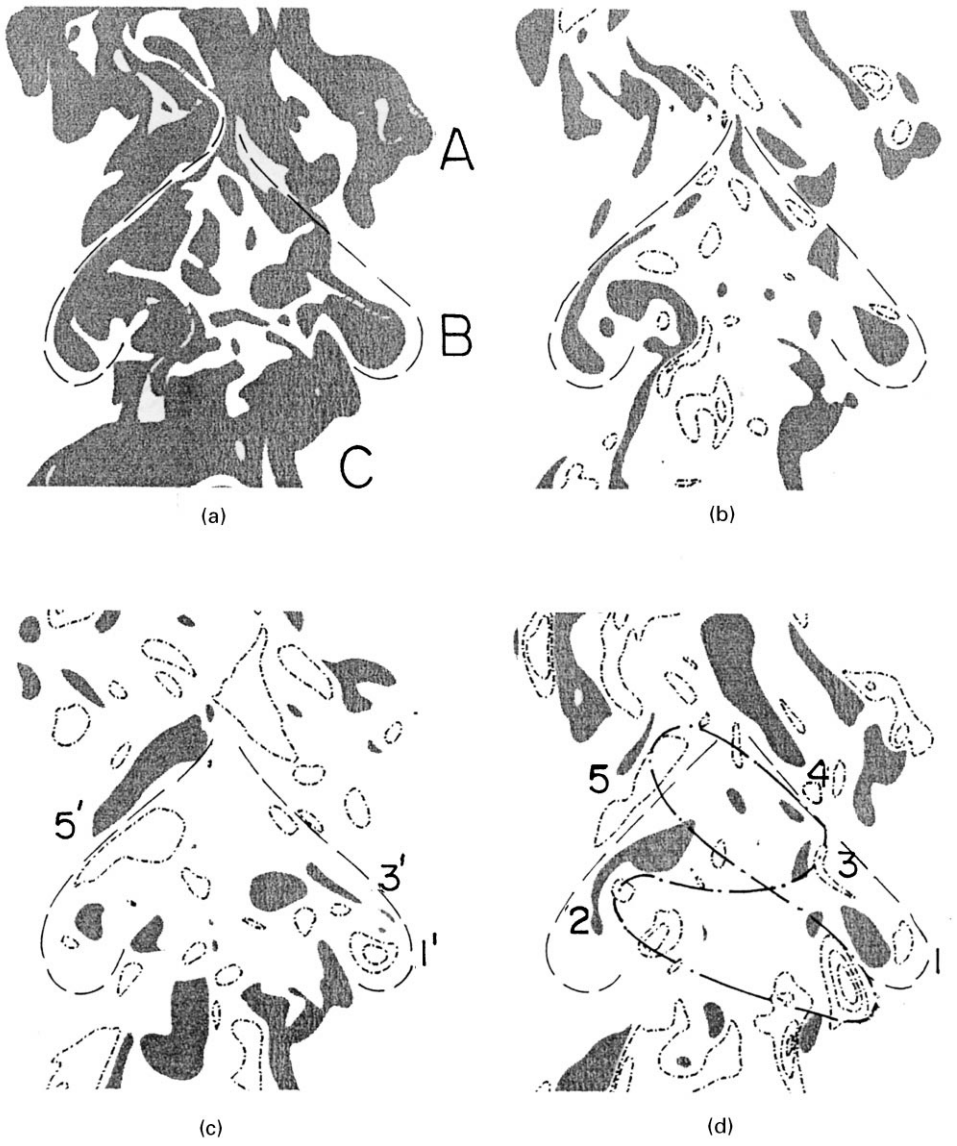

Fig. 5. Magnitude and components of vorticity in the unheated jet at section $X = 65$ and time $t = 35$. (a) Magnitude, (b) Azimuthal component, (c) Radial component, (d) Streamwise component. Solid (dashed line) contours: positive (negative) values.

The heated jet closely resembles the unheated case until $t = 29$. At $t = 29$, structures A′ and B′ in the heated jet are roughly of the same shape and occupy the same streamwise position as their unheated counterparts A and B. By $t = 31$, both A′ and B′ have travelled further downstream than A and B, undoubtedly because of the higher jet velocities following heating. Also, B′ is stretched streamwise compared to B. Structure C′ appears at the bottom of the box. At $t = 35$, A′ can barely

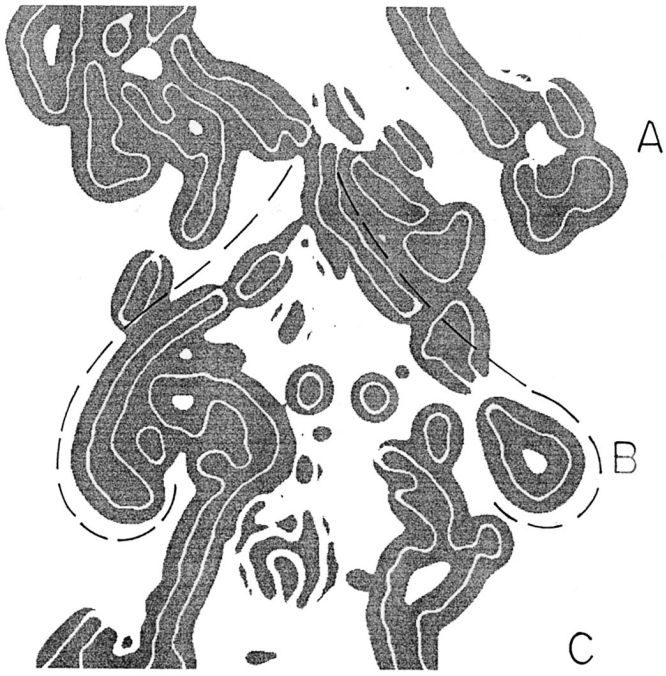

Fig. 6. Wavelet transform of azimuthal vorticity, in the unheated jet at section $X = 65$ and $t = 35$, at wavelet scale $\frac{16}{128}$.

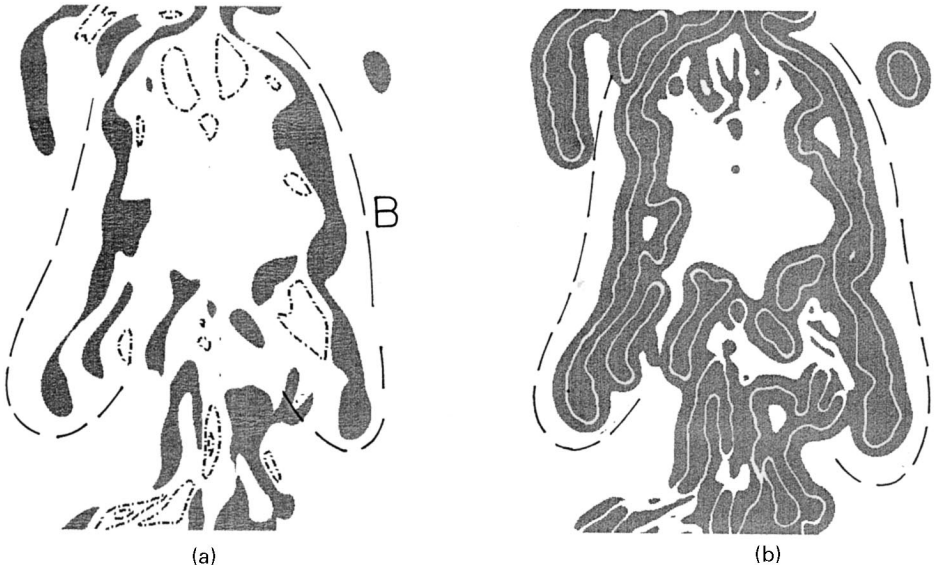

Fig. 7. Section of the unheated jet at $Y = 65$ and time $t = 35$: (a) Azimuthal vorticity, (b) wavelet transform at scale $\frac{16}{128}$.

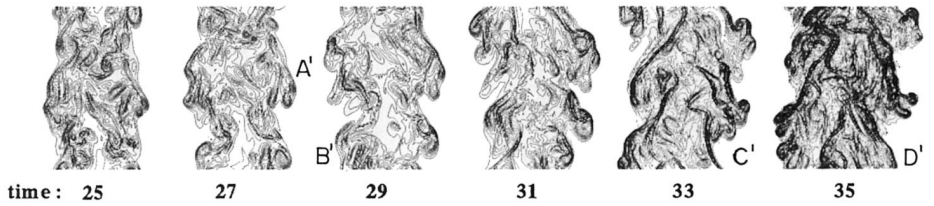

Fig. 8. Evolution of absolute magnitude of vorticity in the heated jet at section $X = 65$ from times $t = 25$ to 35 in steps of two time units. Contour levels start from 1 with increments of 4.

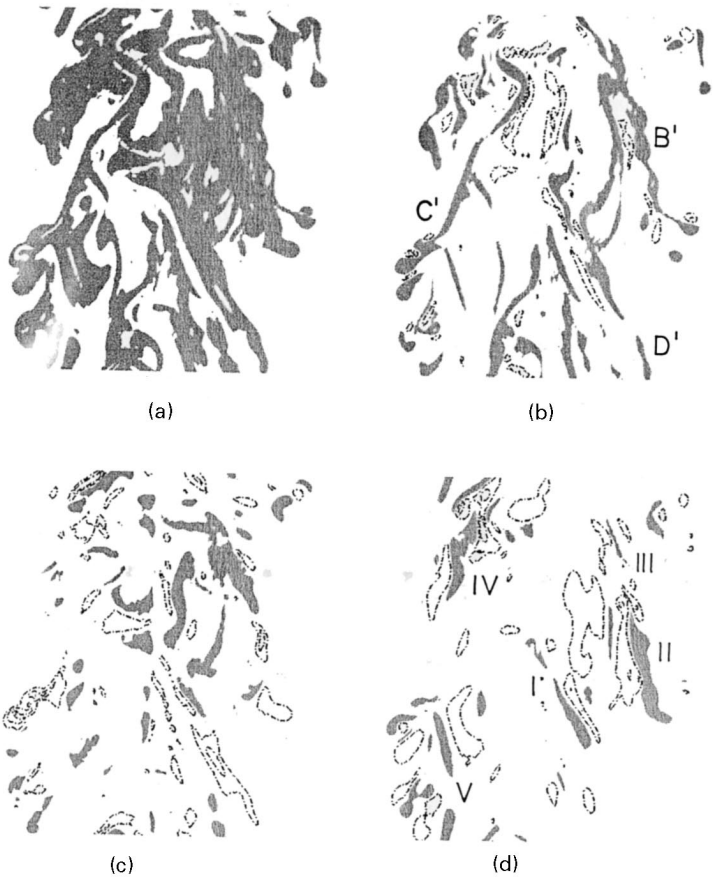

Fig. 9. Magnitude and components of vorticity in the heated jet at section $X = 65$ and time $t = 35$. (a) Magnitude, (b) Azimuthal component, (c) Radial component, (d) Streamwise component. Solid (dashed line) contours: positive (negative) values.

be seen. B′ has accelerated to the top of the domain, but lacks the coherence and continuity of B, breaking down along the sides. Structure C′ has moved to the center of the box, piercing through B′ and disrupting it. A large strip of the positive vorticity of C′ is seen near the jet centerline inside B′. At $t = 35$, the structures are totally disrupted, and can be identified only by the strips of positive

vorticity along their sides. The trailing edge of B′ is seen at the top of the domain, C′ is centrally located and a new structure D′ is creeping up from the bottom of the box.

The sections at $X = 65$ and $t = 35$ of the magnitude of vorticity and its components are shown for the heated jet in Fig. 9. The plots are markedly different from those of the unheated jet at the same time. The azimuthal plot shows the strips on the sides of B′, C′ and the emerging D′. The pairing of positive and negative vorticity seen in the streamwise and radial components of the unheated jet is observed here too, as indicated by areas I through V, all indicating streamwise pairing. But although present, the pairs in the radial plot do not show the correspondence with the streamwise plot that was seen in the unheated case, nor is there any definite order in arrangement.

6. Conclusions

In the present study, we have focussed our attention exclusively on the vorticity field and its components as it is vorticity that defines a coherent structure. In overall shape and size the structures educed in the unheated jet are like the "arrowheads" of Dahm and Dimotakis; thus, the streamwise extent of the structure roughly matches its width. The structure is also comparable to that proposed by Mungal and Hollingsworth — it is roughly axisymmetric with a conical downstream end. But unlike Mungal and Hollingworth's picture (Fig. 2(b)), the present structures telescope negligibly into their downstream counterparts.

Analysis of the components of vorticity reveals large-scale organization mostly in the azimuthal vorticity. A primary structure comprising a torus with a conical sheath of azimuthal vorticity on top and little within the structure is educed. The structure is thus dominated by azimuthal vorticity of the same sign as the initial cylindrical mixing layer.

Apart from this, we also note the presence of a secondary structure, namely the occurence of pairs of streamwise vortex filaments, roughly connecting up into an inclined vortex loop. This loop is unlikely to be a part of the counter-rotating spirals mentioned by Yoda et al., as it is present within the structure and is not of a large-enough scale; the filaments are of a scale about one-tenth the local jet diameter. However, we are unable to comment further upon this matter as our simulation provides us with only one instantaneous structure. What we can say with confidence is that the streamwise vortices noticed in the present simulations cannot be the result of interactions between tilted near-field vortex rings, since we can distinguish these rings; they are tilted, but there is no evidence of interconnection, at least till $t = 35$.

Heating accelerates the flow. Also, the baroclinic torque resulting from the heating enhances the vorticity dramatically. The coherent structures, as a result, get stretched streamwise and run into their downstream counterparts. After prolonged heating, this leads to a complete breakdown of coherent motion.

Acknowledgements

We would like to thank the Jawaharlal Nehru Centre for Advanced Scientific Research for supporting SSS by its Summer Research Fellowship Program. We would also like to thank Mr. I.V.R. Sivakumar for his assistance.

References

Basu, A.J., Narasimha, R., 1999. Direct numerical simulation of turbulent flows with cloud-like off-source heating. J. Fluid. Mech., 385, 199–228.

Bhat, G.S., Narasimha, R., 1996. A volumetrically heated jet: large-eddy structure and entrainment characteristics. J. Fluid Mech. 325, 303–330.

Dahm, W.J.A., Dimotakis, P.E., 1990. Mixing at large Schmidt number in the self-similar far field of turbulent jets. J. Fluid Mech. 217, 299–330.

Dimotakis, P.E., Maike-Lye, R.C., Papanotoniou, D.A., 1983. Structure and dynamics of round turbulent jets. Phys. Fluids 26, 3185–3192.

Elavarasan, R., Bhat, G.S., Narasimha, R., Prabhu, A., 1995. An experimental study of a jet with local buoyancy enhancement. Fluid Dyn. Res. 16, 189–202.

Kailas, S.V., Bhat, G.S., Kalavathi, K., 1992. On coherent structures in a round turbulent jet educed by wavelet transforms. Sixth Asian Congress of Fluid Mechanics.

Kailas, S.V., Narasimha, R., 1999. The eduction of structures from flow imagery using wavelets. Part I. The mixing layer, Expts. Fluids 27, 167–174.

Marr, D., Hildreth, E., 1980. Theory of edge detection. Proc. Roy. Soc. Lond. A 207, 187–217.

Meyer, Y., 1993. Wavelets: Algorithms and Applications. SIAM, Philadelphia.

Mungal, M.G., Hollingsworth, D.K., 1989. Organized motion in a very high Reynolds number jet. Phys. Fluids A1, 1615–1623.

Tso, J., Hussain, F., 1989. Organized motion in a fully developed turbulent axisymmetric jet. J. Fluid Mech. 203, 425–448.

Yoda, M., Hesselink, L., Mungal, M.G., 1994. Instantaneous three-dimensional concentration measurements in the self-similar region of a round high-Schmidt-number jet. J. Fluid Mech. 279, 313–350.